AGU PUBLICATIONS

Geophysical Research Letters

RESEARCH LETTER
10.1002/2016GL071004

Key Points:
- An "attenuation" apparatus has been modified to allow both torsional and flexural oscillation measurements under common P-T conditions
- Reduction of Young's modulus with increasing temperature can be reconciled with shear data, without invoking bulk relaxation
- Flexural and extensional measurements at high homologous temperature provide little resolution of bulk modulus

Correspondence to:
C. J. Cline II,
Christopher.Cline@anu.edu.au

Citation:
Cline, C. J., II, and I. Jackson (2016), Relaxation of the bulk modulus in partially molten dunite?, *Geophys. Res. Lett.*, *43*, 11,644–11,651, doi:10.1002/2016GL071004.

Received 26 AUG 2016
Accepted 10 NOV 2016
Accepted article online 12 NOV 2016
Published online 26 NOV 2016

Relaxation of the bulk modulus in partially molten dunite?

C. J. Cline II[1] and I. Jackson[1]

[1]Research School of Earth Sciences, Australian National University, Canberra, ACT, Australia

Abstract To address the possibility of melt-related bulk modulus relaxation, a forced oscillation experiment was conducted at seismic frequencies on a partially molten synthetic dunite specimen (melt fraction = 0.026) utilizing the enhanced capacity of the Australian National University attenuation apparatus to operate in both torsional and flexural oscillation modes. Shear modulus and dissipation data are consistent with those for melt-bearing olivine specimens previously tested in torsion, with a pronounced dissipation peak superimposed on high-temperature background. Flexural data exhibit a monotonic decrease in complex Young's modulus with increasing temperature under transsolidus temperatures. The observed variation of Young's modulus is well described by the relationship $1/E \sim 1/3G$, without requiring relaxation of the bulk modulus. At high homologous temperatures, when shear modulus is low, extensional and flexural oscillation measurements have little resolution of bulk modulus, and thus, only pressure oscillation measurements can definitively constrain bulk properties at these conditions.

1. Introduction

Obtaining a robust experimental understanding of viscoelastic properties in partially molten dunite underpins the ability to invert seismic attenuation profiles [e.g., *Romanowicz and Mitchell*, 2015] into meaningful representations of melt content and its distribution within the Earth's upper mantle. The relaxation characteristics, and more importantly the inferred mechanism of dissipation in partially molten aggregates, vary between experimental and theoretical studies. Experimental observations of *Gribb and Cooper* [2000] on partially molten olivine show a decrease in shear modulus and concomitant increase in the high-temperature background (HTB) signal at supersolidus temperatures. In contrast, *Jackson et al.* [2004] reported a conspicuous qualitative change in the absorption band above the solidus, with a large melt-related peak superimposed upon the HTB. In neither case was there clear evidence that melt distributed mainly in the classic equilibrium texture (confined to grain-edge tubules by surface tension) has the capacity to explain the observed large changes of shear properties [*Waff and Bulau*, 1979; *Mavko and Nur*, 1975]. Moreover, these experimental studies were confined to torsional oscillation, without data from complimentary modes of oscillation that could investigate bulk properties. *Li and Weidner* [2013] conducted extensional (longitudinal) mode forced oscillation experiments on partially molten peridotite and proposed both bulk (K) and shear (G) modulus relaxation through modification of phase proportions (liquid and solid) in response to transient perturbations from local thermodynamic equilibrium, as expected with passing seismic waves. These outstanding experimental discrepancies, in combination with the above obtaining data solely for complex shear (G^*) or complex Young's modulus (E^*), thus necessitate further experimentation that can probe the full relaxation spectrum of rocks containing partial melts, involving measurements of both G and E, allowing the theoretical inference of K and any associated deviation from anharmonic behavior.

Using the newly developed capability of the Australian National University (ANU) attenuation apparatus, which allows interrogation of specimens under both forced torsional and flexural oscillation at seismic frequencies and high temperature, we report the first detailed analysis of E^* and G^* in dunite under transsolidus conditions. This provides the possibility, in principle, to address bulk modulus dissipation through stress-driven melt redistribution and/or stress-induced alterations of liquid-solid phase proportions and thus the implications for both compressional and shear waves.

2. Methodology

2.1. Specimen Fabrication and Mechanical Testing

The synthetic dunite specimen was fabricated using the methodology of *Faul et al.* [2004] by mixing pure sol-gel-derived Fo90 olivine powder with 3.5 wt % pulverized basaltic glass in an agate mortar and pestle

(solidus ~ 1150°C [from *Faul et al*., 2004]). The mixed powder was pelletized and sintered at 1300°C for 16 h under controlled atmosphere. The pellets were then wrapped in Ni/Fe foil and hot pressed using an internally heated Paterson gas-medium apparatus at 300 MPa and 1300°C for 24 h to produce a near fully dense aggregate. Scanning electron microscope imaging shows that melt distribution in this aggregate is similar to the study of *Faul et al*. [2004], with melt homogenously distributed throughout the specimen, possessing no observed radial gradients in concentration, and with melt being primarily located at triple and quadruple junctions. Average melt fraction of the recovered specimen is calculated at 0.026 using binary image analysis, with a section-corrected average grain diameter of 19.9 μm. Fourier transform infrared spectra collected on a 400 μm thick slab show no appreciable absorption above background for either olivine grains or basaltic melt between the wave numbers 4000 and 3000 cm^{-1} (associated with O-H bonding); thus, we can conclude that the experiment was conducted under fully anhydrous conditions.

The hot-pressed specimen was precision ground to cylindrical shape, wrapped in Ni/Fe foil, inserted into a mild steel jacket, and sandwiched between a series of optically flat Lucalox™ alumina pistons [*Jackson et al*., 2009]. This jacketed assembly was then affixed inside of a modified Paterson gas apparatus used for the high-temperature oscillatory mechanical test [*Jackson and Paterson*, 1993]. Confining pressure was increased to 200 MPa, and then temperature was raised to the targeted maximum testing temperature (1300°C), and the specimen was annealed for approximately 48 h. During this time the torsional response of the specimen was continually monitored for any temporal evolution of the modulus and dissipation. Once the mechanical response had stabilized, linearity was confirmed for maximum strain amplitudes $< 5 \times 10^{-5}$ by variation of the strain amplitude before the start of the formal experiment.

Mechanical testing was conducted using both forced torsional and flexural oscillation at a series of 10 logarithmically equispaced periods between 1 and 1000 s. At 1300°C the specimen was first interrogated in torsional oscillation; thereafter, the electromagnetic drivers and displacement transducers were electronically switched to flexural mode and the series of tests is repeated using an oscillatory bending force (Figure 1). Upon completion of both torsional and flexural oscillation tests, the temperature was dropped in 50°C intervals down to room temperature, with the full suite of tests being conducted at each temperature interval.

2.2. Enhanced Capability for Flexural Oscillation Measurements

Recognizing the value of low-frequency laboratory constraints on both shear and compressional wave properties, we have modified our attenuation apparatus, previously used exclusively in torsional mode, to allow complementary flexural oscillation measurements. Initially, such flexural measurements, involving an oscillating bending moment applied about a horizontal axis near the lower end of the vertically oriented experimental assembly, required the rotation of both electromagnetic driver units and displacement transducers through 90° from the orientation employed for torsional oscillation [*Jackson et al*., 2011] (Figures 1a and 1b). However, it is operationally more convenient to study both torsional and flexural oscillation under identical environmental conditions without having to cool and depressurize to change the driver and transducer polarizations. Accordingly, we have increased the clearance at the lower end of the assembly so that it is now cantilevered within the pressure vessel via a torsionally and flexurally compliant spiral vent tube (Figure 1c). This modified assembly is subjected to a horizontally polarized oscillating bending force, rather than the previously described bending moment. Remote manipulation of alternative electrical connections allows generation of either an oscillating torque or bending force and measurement of the torsional or flexural modes without alteration of driver/detector geometry (Figure 1c).

The interim results from such flexural oscillation measurements are presented as the distortion of the entire specimen assembly comprising the jacketed specimen and connecting rods and the hollow steel members between which they are sandwiched. d^*_1, the complex flexural mode displacement measured at the upper measurement station and reflecting the distortion of the specimen assembly, is compared with that (d^*_{12}) of the elastic element located between the upper and lower displacement measurement stations, by defining a complex normalized flexural "modulus" S^*_{nf} as

$$S^*_{nf} = \frac{d^*_1}{d^*_{12}} = \frac{d^*_1}{d^*_2 - d^*_1} = S_{nf}\exp(-i\delta) \tag{1}$$

where the loss angle δ (rad) is the phase lag of d^*_1 relative to d^*_{12}, associated with strain energy dissipation. For an example of raw flexural oscillation displacement data, refer to *Jackson et al*. [2011].

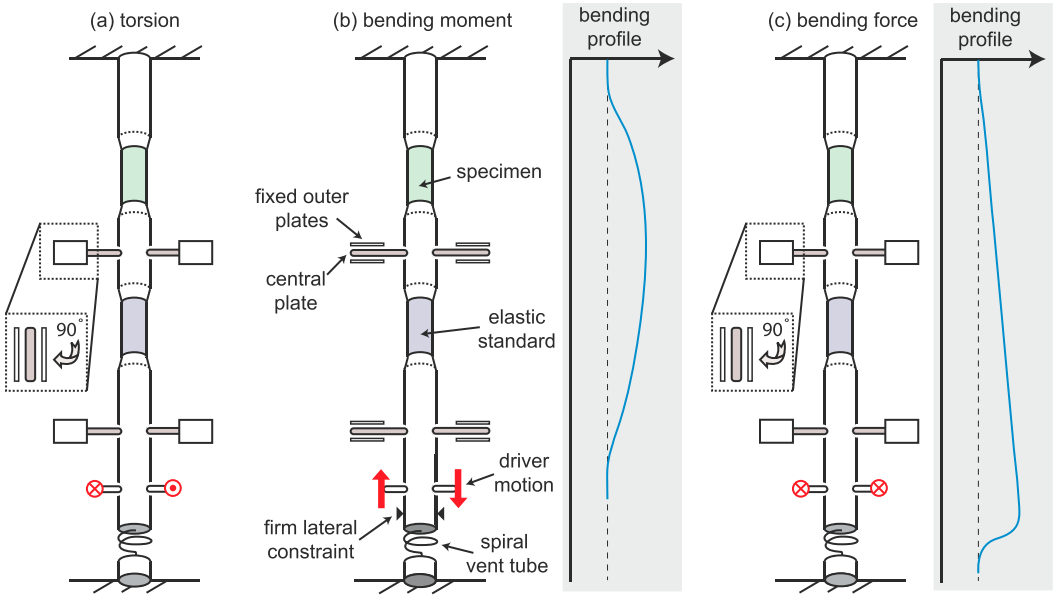

Figure 1. The driver and detector geometries in both torsional and flexural data collection modes. (a) Torsion: the motion, alternately into and out of the page, of the central capacitance plates relative to their respective outer pairs of fixed plates, is measured with parallel combinations of individual capacitors (diagonally opposed in plan view); electromagnetic driver motion is similarly polarized. (b) Previous flexural arrangement described by *Jackson et al.* [2011]. Drivers and detector plates have been rotated 90° from Figure 1a in order to generate a bending moment and measure displacement associated with the resulting flexure in the plane of the page. (c) Flexural arrangement in current study. Detector plates and drivers maintain the same geometry as torsional measurements, but drivers act in combination alternately both into and out of the plane of page to produce a bending force normal to the page rather than a torque, with parallel combinations of individual capacitors, directly opposed in plan view. The short compliant spiral vent tube now participates in the flexure of the doubly cantilevered beam.

2.3. Modeling the Flexural Response

We have previously demonstrated the adequacy of the filament elongation model for describing the elastic flexural response of a compound long thin beam with the dimensions and material properties of the experimental assembly [*Jackson et al.*, 2011]. Here we highlight changes required for the incorporation of high-temperature viscoelastic behavior into the now doubly cantilevered assembly [*Timoshenko and Gere*, 1990]. Within a right-handed coordinate system, the static lateral deflection $v(x) \parallel y$ of the long thin model beam ($0 < x < L$) is controlled by the extension/contraction of its constituent longitudinal filaments through the differential equation

$$\partial^2 v/\partial x^2 = M(x)/E(x)I(x) \tag{2}$$

[*Timoshenko and Gere*, 1990]. E and I are, respectively, the Young's modulus and the diametral moment of inertia of the beam's cross-section $\perp x$, and M measured clockwise around $+z$ is the local bending moment. A finite-difference approximation to equation (2) involves division of the length L of the entire experimental assembly into a series of N small intervals (x_{i-1}, x_i) $(i = 1, N_S)$ each of the same width $h = L/N$. With the flexural rigidity $(EI)_i = E(x_i)I(x_i)$, local bending moment $M_i = M(x_i)$, and deflection $v_i = v(x_i)$, specified at each of the x_i $(i = 0, N)$, the governing equation becomes

$$v_{i-1} - 2v_i + v_{i+1} = \frac{h^2 M_i}{(EI)_i}, i = 0, N. \tag{3}$$

M_i is related to the bending force F applied at $x = l_3$, the terminal reaction force R_L, and terminal bending moment M_L at the lower end of the beam ($x = L$), through an analysis of static equilibrium:

$$M_i = R_L(L - x_i) + F(l_3 - x_i) + M_L \text{ for } 0 \le x_i < l_3$$
$$\text{and} \tag{4}$$
$$M_i = R_L(L - x_i) + M_L \text{ for } l_3 < x_i \le L$$

The cantilevered boundary conditions at either end of the beam imply that $v_0 = v(x_0) = v_N = v(x_N) = 0$ and that $v'(x_0) = (v_1 - v_{-1})/2h = 0 = v'(x_N) = (v_{N+1} - v_{N-1})/2h$.

The temperature gradient along the assembly is approximated as a series of connected linear segments spanning the temperature range between room temperature and the maximum temperature (T) of the hot zone within the internal furnace. High-temperature viscoelasticity of the specimen, polycrystalline alumina connecting rods and jacket are incorporated through E^*, specified in terms of the corresponding G^* and K^* for the appropriate oscillation period, using the relation

$$\frac{1}{E^*} = \frac{1}{3G^*} + \frac{1}{9K^*} \tag{5}$$

Application of the boundary conditions, along with separation of the real and imaginary parts of equations (3), results in a linear system $Av = B$ comprising $2(N+1)$ equations in the same number of components of the solution vector.

The standard method of linear decomposition [*Press et al.*, 1986] is used to solve for the real and imaginary parts of the deflection v_i ($i = 1, N-1$) and of the statically indeterminate quantities R_L and M_L. For comparison with the experimentally determined normalized flexural modulus, we extract from the results of the finite-difference modeling the corresponding quantity

$$S^*_{\mathrm{mod}} = \frac{v(l_1)}{v(l_2) - v(l_1)} = S_{\mathrm{mod}} \exp(-i\delta_{\mathrm{mod}}) \tag{6}$$

where l_1 and l_2 are the values of coordinate x for the displacement measurement stations located above and below the steel elastic standard (Figure 1). The spiral vent tube at the lower end of the experimental assembly is modeled as a straight tube of the same length and internal diameter with an effective outer diameter predetermined by modeling the flexure of an assembly containing an elastic control specimen of single-crystal sapphire.

3. Results

The torsional oscillation data for the partially molten specimen are processed in the usual way [*Jackson et al.*, 2009] to obtain the variations of shear modulus (G) and dissipation (Q^{-1}) with oscillation period (T_o) and temperature (T) (Figure 2). This procedure involves Fourier transformation of raw sinusoidal time series data to obtain the normalized torsional compliance (cf. equation (1)) for the specimen assembly. Comparison with the corresponding quantity for a geometrically similar elastic reference assembly allows determination of shear modulus and dissipation for the specimen itself. A correction has been made to account for the presence of melt layers of ~50 μm thickness resulting from chemical reaction between the olivine specimen and adjacent alumina pistons. The torsional compliance of the terminal melt layers has been modeled with a single layer within the assembly having a thermally activated viscosity ranging from ~1 Pa s at 1300°C to >100 Pa s below 1200°C. The magnitude of this correction is small, reducing the determined values of G and Q^{-1} by less than 1% at supersolidus conditions ($T \geq 1100$°C). Torsional data show similar behavior to that previously described in *Jackson et al.* [2004] for melt-bearing olivine, with a pronounced dissipation peak superimposed upon a high-temperature background creating a dissipation "plateau" within the 1–1000 s observational window in the temperature range 1100–1200°C (Figure 2b). The data are similarly reasonably well described by an extended Burgers model inclusive of background and peak (Figure 2) [*Jackson and Faul*, 2010; *Jackson*, 2015].

The complex shear modulus $G^*(T_o, T)$, thus determined, is combined with the (real) anharmonic value of bulk modulus ($K(T)$) to estimate $E^*(T_o, T)$ through equation (5). The results of such modeling are compared with the flexural oscillation observations, expressed in terms of normalized flexural modulus and phase lag, as determined from the Fourier transformed sinusoidal displacement data (Figure 3). The parallel configuration of capacitance displacement transducers for the torsional mode discriminates strongly against the mainly flexural disturbance of the specimen assembly by the dense gas pressure medium undergoing vigorous thermal convection [*Jackson and Paterson*, 1993]. However, such discrimination against flexural noise is unavailable for the corresponding flexural mode measurements—resulting in increased scatter, especially of the small phase lags. The possibility of using the filament elongation model to characterize and subtract such flexural mode mechanical noise is deferred for future attention.

Model results obtained using anharmonic values of K accurately predict the frequency dependence of experimental flexural modulus and generally exhibit the correct temperature sensitivity (Figure 3a). The largest

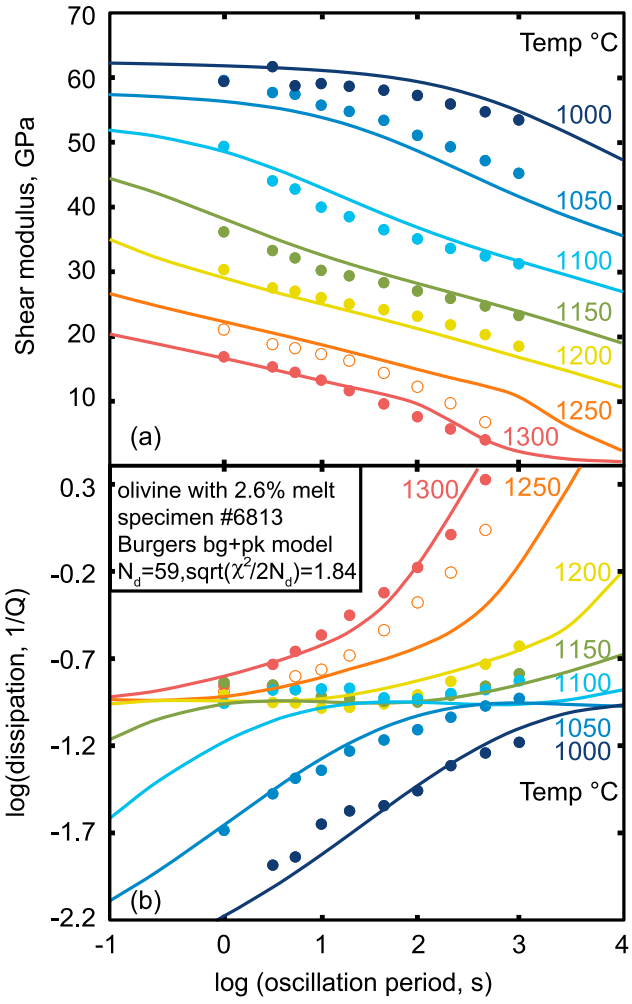

Figure 2. Torsional oscillation data for melt-bearing olivine specimen #6813 versus oscillation period and temperature. Circles indicate data points, while the curves represent the extended Burgers model inclusive of background and superimposed peak, fitted to N_d (G, Q^{-1}) pairs—being all data for 1000–1300°C exclusive of those at 1250°C denoted by open symbols. (a) Shear modulus and (b) dissipation.

discrepancy is observed in the temperature range associated with the dissipation peak in the torsional data set, with the model compliance being greater than that of the partially molten dunite, providing no scope to increase the quality of the fit by relaxation of K in this temperature range (i.e., equation (5)). Phase lag data are low in overall magnitude; thus, signal/noise ratios in observed experimental values obscure the clear trends of temperature and frequency dependence of the data at intermediate temperatures (Figure 3b). Despite the noisy phase lag data, the observed temperature and limited frequency dependence is also adequately captured by use of anharmonic (real) K and G^* in the calculation of E^*.

4. Discussion and Conclusion

4.1. Compressive Mode Viscoelasticity: K^*?

Here we have provided novel seismic-frequency data collected in both torsional and flexural modes to address the possibility of bulk modulus relaxation in partially molten dunite. Using the complex shear modulus as a constraint, we have demonstrated that no deviation from anharmonic (real) K is required to match the temperature and frequency dependence of E^* inferred from flexural measurements. Under these conditions of low shear modulus, E^* is insensitive to variations in K; as suggested by *McCarthy and Takei* [2011, equation (6)], equation (5) can be approximated as $1/E \sim 1/3G$, as the contribution of the $1/9$ K component is numerically insignificant. Demonstrating this consistency, we compare $|E^*|$ (inferred from flexural measurements with anharmonic K) to $3|G^*|$ from torsional measurements (Figure 4a). The values of $|E^*|$ and $3|G^*|$ are essentially indistinguishable for supersolidus conditions, both decreasing consistently with increasing temperature.

Moreover, the variation of $|E^*|$ across transsolidus conditions in our study is closely consistent with the variation of $|E^*|$ with pressure (i.e., melt fraction/productivity) in extensional oscillation measurements on a partially molten lherzolite [*Li and Weidner*, 2013] (Figure 4b) suggesting a common relaxation mechanism. *Li and Weidner* [2013] associated their observed pressure dependence of E (Figure 4b) with the predicted effects of "dynamic melting," i.e., stress-induced changes of melt fraction, on both bulk and shear moduli. However, it is evident from the results of the present study that their measurements would, in fact, have been insensitive to any such relaxation of the bulk modulus.

Given the relation between E and G reexpressed as $E = 3G/[1 + (G/3K)]$, it is apparent that at low values of G ($G/3K << 1$), there is little resolution of K when measuring E by means of flexural, or more commonly employed

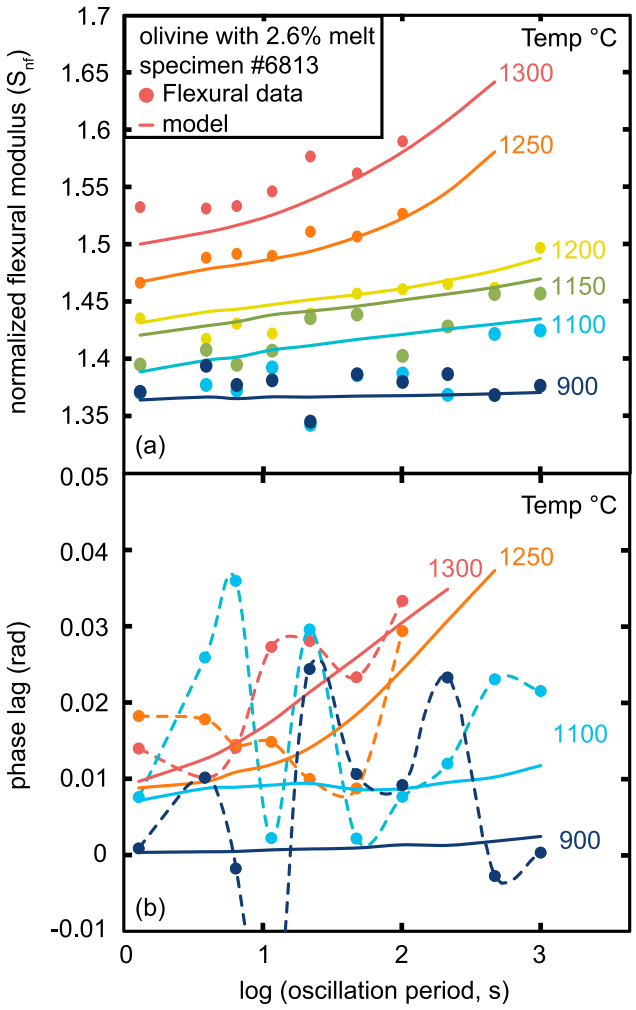

Figure 3. Flexural oscillation data for melt-bearing specimen #6813 plotted versus temperature. Filled circles indicate observed flexural data, while solid curves represent the flexural model evaluated with G^* from torsional oscillation (Figure 2) and anharmonic K. (a) Normalized flexural modulus (S_{nf}) of the specimen assembly and (b) phase lag data for representative temperatures for visual clarity, but results shown are representative of the entire data set.

longitudinal, mode oscillation [e.g., *Takei et al.*, 2014]. Only as the temperature decreases and shear modulus increases is there a significant difference between $|E^*|$ and $3|G^*|$, providing the potential to resolve variations in K^* (Figure 4). These findings suggest that at high homologous temperatures (inclusive of supersolidus conditions), when shear modulus is comparatively low, oscillation of pressure rather than bending force or uniaxial stress might be required for the robust measurement of K^*, as in the work by *Pimienta et al.* [2015] on fluid-saturated porous media at room temperature.

Although relaxation of the bulk modulus is evidently not required to reconcile E^* and G^* measured at high homologous temperatures, such relaxation cannot be excluded. There is simply insufficient sensitivity in flexural or extensional/longitudinal oscillation methods to observe such a phenomenon. Plausible causes of bulk modulus relaxation include stress-induced variations of melt fraction [e.g., *Li and Weidner*, 2013] and stress-induced specimen-wide redistribution of melt. Such mesoscale melt flow may be expected during our flexural oscillation tests (especially in the terminal melt layers) between the side of the specimen instantaneously in compression to the other side in tension, as well as during extensional oscillation between the specimen interior and an external reservoir (i.e., draining). At lower temperatures, with better resolution of K in flexural measurements, it may be possible that solid-state phase transformations between coexisting phases of contrasting density could be observed to provide bulk modulus attenuation [*Li*, 2010; *Ricard et al.*, 2009], providing another avenue of potential experimentation utilizing our new capability for high-temperature flexural oscillation measurements.

4.2. Shear Mode Viscoelasticity: G^*

Shear attenuation and associated modulus dispersion are strongly affected by the presence of melt in all seismic-frequency measurements conducted within the ANU lab—with the consistent observation of a dissipation peak superimposed upon the usual monotonic background. With no reported evidence for grain boundary melt layers of sufficiently low aspect ratio ($<10^{-2}$), the peak was previously attributed to elastically accommodated grain boundary sliding [*Faul et al.*, 2004]. However, recent serial sectioning studies of partially molten olivine suggest that melt not only is present in grain-edge tubules but also wets a significant proportion of olivine grain boundaries with melt layers of ~10–100 nm thickness, providing aspect ratios of $\sim 10^{-3}$ [*Garapić et al.*, 2013].

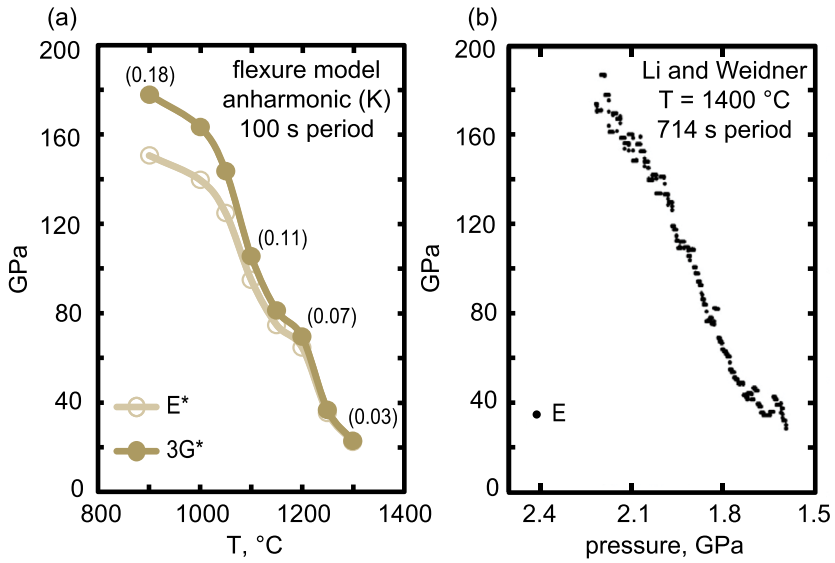

Figure 4. (a) The modulus of the complex Young's modulus (E^*) calculated using previously collected complex shear modulus (G^*) data in combination with anharmonic values of real bulk modulus at 100 s oscillation period plotted against temperature ranging from subsolidus to supersolidus conditions. Also plotted is the quantity $3|G^*|$, showing that the relation described by equation (5) can be approximated as $1/E \sim 1/3G$, and softening of E is well described without requiring a partially relaxed K. Values of G/3 K are indicated at selected temperatures in parenthesis. (b) Young's modulus as a function of pressure (melt fraction) for a partially molten lherzolite (modified after *Li and Weidner* [2013]). Melt fraction variation through the temperature interval represented in Figure 4a is similar to the melt fraction change as a function of pressure in Figure 4b, with a reported maximum melt fraction of ~3–4%.

Under an externally imposed shear stress, melt squirt is driven by a pressure differential between adjacent parts of a melt network, which differ in their effective compliance because of different aspect ratios (e.g., thin melt layers versus grain-edge tubules) and/or different orientations relative to the stress field (e.g., layers parallel or normal to the principal compressive stress). For dynamic melting to contribute to shear modulus relaxation, it is required that the local pressure differential be sustained, i.e., be unrelaxed by melt squirt, during the period of the oscillating stress—conditions diagnostic of the saturated isolated regime [*O'Connell and Budiansky*, 1977]. Conditions transitional between the saturated isolated and saturated isobaric regimes, potentially favorable for relaxation by dynamic melting and/or melt squirt within the observational window (1100–1300°C, 1–1000 s period) for our torsional mode experiments (Figure 2), may be identified as follows. The characteristic time for squirt of melt of viscosity η between ellipsoidal inclusions of aspect ratio α is $\tau = 2\pi\eta/K_s\alpha^3$, where K_s is the bulk modulus of the solid matrix [*O'Connell and Budiansky*, 1977]. Values of α in the range $10^{-3.5}$–$10^{-2.5}$, consistent with the observations of thin melt layers by *Garapić et al*. [2013], along with basaltic melt viscosities appropriate for near-solidus temperatures, yield squirt relaxation times within the seismic band, confirming that melt squirt is a plausible relaxation mechanism [*Faul and Jackson*, 2015]. Shear modulus relaxation by dynamic melting model requires that the timescale for stress-induced melt squirt exceeds that for stress-induced change of melt fraction. However, the persistence of glass in specimens relatively slowly cooled in our hot-pressing and mechanical testing experiments suggests that the melting/crystallization process may be too slow under near-solidus conditions to meet this criterion.

Acknowledgments
The authors would like to thank Ulrich Faul for helpful discussions in experiment design, along with Harri Kokkonen and Hayden Miller for technical support in specimen preparation and characterization, along with the operation of the rock physics high-pressure laboratory. This work was supported by grant DP130103848 from the Australian Research Council to I.J., and C.J.C. II gratefully acknowledges funding through the ANU International PhD Research Scholarship. Additionally, the authors would like to Yasuko Takei and Christine McCarthy for their thoughtful comments on the manuscript. All data presented in this manuscript are available through e-mail with the corresponding author C.J.C. (Christopher.cline@anu.edu.au).

References

Faul, U., and I. Jackson (2015), Transient creep and strain energy dissipation: An experimental perspective, *Annu. Rev. Earth Planet. Sci.*, *43*, 18.1.

Faul, U. H., J. D. Fitz Gerald, and I. Jackson (2004), Shear wave attenuation and dispersion in melt-bearing olivine polycrystals: 2. Microstructural interpretation and seismological implications, *J. Geophys. Res.*, *109*, B06202, doi:10.1029/2003JB002407.

Garapić, G., U. Faul, and E. Brisson (2013), High-resolution imaging of the melt distribution in partially molten upper mantle rocks: Evidence for wetted two-grain boundaries, *Geochem. Geophys. Geosyst.*, *14*, 556–566, doi:10.1029/2012GC004547.

Gribb, T. T., and R. F. Cooper (2000), The effect of an equilibrated melt phase on the shear creep and attenuation behavior of polycrystalline olivine, *Geophys. Res. Lett.*, *27*(15), 2341–2344, doi:10.1029/2000GL011443.

Jackson, I. (2015), 2.21—Properties of pocks and minerals: Physical origins of anelasticity and attenuation in rock, in *Treatise on Geophysics*, 2nd ed., edited by G. Schubert, pp. 539–571, Elsevier, Oxford.

Jackson, I., and U. H. Faul (2010), Grain size-sensitive viscoelastic relaxation in olivine: Towards a robust laboratory-based model for seismological application, *Phys. Earth Planet. Inter.*, *183*(1–2), 151–163.

Jackson, I., and M. S. Paterson (1993), A high-pressure, high-temperature apparatus for studies of seismic wave dispersion and attenuation, *Pageoph*, *141*(2–4), 445–466.

Jackson, I., U. H. Faul, J. D. Fitz Gerald, and B. H. Tan (2004), Shear wave attenuation and dispersion in melt-bearing olivine polycrystals: 1. Specimen fabrication and mechanical testing, *J. Geophys. Res.*, *109*, B06201, doi:10.1029/2003JB002406.

Jackson, I., A. Barnhoorn, Y. Aizawa, and C. Saint (2009), Improved procedures for the laboratory study of high-temperature viscoelastic relaxation, *Phys. Earth Planet. Inter.*, *172*(1–2), 104–115.

Jackson, I., H. Schijns, D. R. Schmitt, J. Mu, and A. Delmenico (2011), A versatile facility for laboratory studies of viscoelastic and poroelastic behaviour of rocks, *Rev. Sci. Instrum.*, *82*(6), 064501.

Li, L. (2010), Bulk attenuation in the Earth's mantle due to phase transitions, *Phys. Earth Planet. Inter.*, *183*(3–4), 473–477.

Li, L., and D. J. Weidner (2013), Effect of dynamic melting on acoustic velocities in a partially molten peridotite, *Phys. Earth Planet. Inter.*, *222*, 1–7.

Mavko, G., and A. Nur (1975), Melt squirt in the asthenosphere, *J. Geophys. Res.*, *80*(11), 1444–1448, doi:10.1029/JB080i011p01444.

McCarthy, C., and Y. Takei (2011), Anelasticity and viscosity of partially molten rock analogue: Toward seismic detection of small quantities of melt, *Geophys. Res. Lett.*, *38*, L18306, doi:10.1029/2011GL048776.

O'Connell, R. J., and B. Budiansky (1977), Viscoelastic properties of fluid-saturated cracked solids, *J. Geophys. Res.*, *82*(36), 5719–5735, doi:10.1029/JB082i036p05719.

Pimienta, L., J. Fortin, and Y. Guéguen (2015), Bulk modulus dispersion and attenuation in sandstones, *Geophysics*, *80*(2), D111–D127.

Press, W. H., B. P. Flannery, S. A. Teukolsky, and W. T. Vetterling (1986), *Numerical Recipes: The Art of Scientific Computing*, Cambridge Univ. Press, Cambridge, Mass.

Ricard, Y., J. Matas, and F. Chambat (2009), Seismic attenuation in a phase change coexistence loop, *Phys. Earth Planet. Inter.*, *176*(1–2), 124–131.

Romanowicz, B. A., and B. J. Mitchell (2015), Deep Earth structure: Q of the Earth from crust to core, in *Treatise on Geophysics*, 2nd ed., edited by G. Schubert, pp. 789–827, Elsevier, Oxford.

Takei, Y., F. Karasawa, and H. Yamauchi (2014), Temperature, grain size, and chemical controls on polycrystal anelasticity over a broad frequency range extending into the seismic range, *J. Geophys. Res. Solid Earth*, *119*, 5414–5443, doi:10.1002/2014JB011146.

Timoshenko, S. P., and J. M. Gere (1990), *Mechanics of Materials PWS*, KENT Publishing Company, Elsevier Sci. BV, Amsterdam.

Waff, H., and J. R. Bulau (1979), Equilibrium fluid distribution in an ultramafic partial melt under hydrostatic stress conditions, *J. Geophys. Res.*, *84*(B11), 6109–6114, doi:10.1029/JB084iB11p06109.